Temporally transitional mantle convection: Implications for Mars

Alexander Loddoch[1,2] and Ulrich Hansen[1]

[1]   The thermal evolution of terrestrial planets such as Earth, Mars, and Venus is strongly dominated by the convective processes in the planet's silicate mantle. The actual style of convection controls the efficiency of heat transport and thus the cooling behavior of the whole planet. In the present study we investigate the heat transport properties of variable viscosity convection, focusing on the temporally transitional behavior discovered recently. While the difference of the newly found convective regime to the already known stagnant lid and episodic behavior has been elaborated in our previous study, the present work investigates the applicability of the observed intermittent behavior to the thermal evolution of terrestrial planets. A 3-D numerical mantle convection code is applied and calculations are carried out in the parameter range for which the temporally transitional behavior has been found. Using the described approach, it is possible to investigate the transition from a (temporarily) mobilized to a stagnant surface in a fluid dynamically consistent manner. While such a scenario has been suggested for Mars' early history, it has so far been investigated only by means of parameterized convection models. We show that the sporadic surface mobilization events may indeed occur on time scales relevant for Mars. In order to assess their influence on the subsequent thermal evolution of planetary bodies, an internal heating of the mantle and a secular cooling of the core are additionally taken into account. The obtained results are compared to the findings of thermal evolution studies employing parameterized convection models. We show that the thermal consequences of a temporal transition from a mobile to a stagnant surface are indeed correctly described by parameterized models as done in previous studies.

1. Introduction

[2] The heat budget of a terrestrial planet like Earth, Mars, or Venus is controlled mainly by thermal convection in the mantle. The actual style of convection (e.g., whether or not the planet shows plate tectonics) has, consequently, a strong influence on the thermal evolution of the whole planet. Active plate tectonics transports hot material close to the cold surface of the planet, thus removing large amounts of heat from the planet's interior. Similarly, the cold subducted surface material efficiently cools the lower parts of the mantle. In contrast, on a planet lacking plate tectonics the heat being transported upward by convection has to pass the immobile crustal layer purely by conduction. Conduction is a far less efficient heat transport mechanism, a planet without plate tectonics will, therefore, remain at higher internal temperatures. Apart form advancing the understanding of plate tectonics as observed on Earth, investigations of mantle convection are hence to be consid-

ered in terms of the thermal evolution of terrestrial planets in general. In fact, numerical studies have shown that for rheologies and parameter values relevant for terrestrial planets, mantle convection manifests in one of three distinct styles [*Moresi and Solomatov*, 1998; *Stein et al.*, 2004]. These are referred to as mobile lid convection, stagnant lid convection, and, in between these two, the episodic behavior corresponding to the respective surface behavior observed. The episodic regime, with a repeated mobilization of the surface, has been considered as being representative for Venus and its (multiple?) global resurfacing events [*Turcotte*, 1993; *Fowler and O'Brien*, 1996; *Turcotte et al.*, 1999]. For Mars, no evidence for recent plate tectonic activity is found and the planet is, therefore, believed to be in the stagnant lid mode of convection [*Schubert and Spohn*, 1990; *Spohn*, 1991]. The mobile lid regime is characterized by a constantly mobilized surface and, therefore, forms the basis for fluid dynamical investigations of plate tectonics as observed on Earth [*Stein et al.*, 2004; *Tackley*, 2000a, 2000b] (see above).

[3] In fluid dynamical investigations the individual convective regimes are typically considered to represent (quasi) steady states. For each set of parameters the system exhibits exactly one style of convection throughout time. Transitions between regimes are possible only in terms of variations of

[1]Institute for Geophysics, University of Münster, Münster, Germany.
[2]Now at Chevron Energy Technology Company, Technical Computing, Houston, Texas, USA.

the controlling parameters such as the Rayleigh number, the strength of temperature dependence of viscosity, or the yield stress. *Stein et al.* [2004] systematically investigated the influence of different parameters on the style of convection and mapped the boundaries between neighboring regimes in parameter space. In our preceding work [*Loddoch et al.*, 2006] we showed that transitions between regimes may also occur temporally, for a fixed set of parameters. Convective systems have been observed in which quasi steady state stagnant lid convection is repeatedly interrupted by sporadic surface mobilization events occurring out of a thermally equilibrated state or is, moreover, completely replaced by an episodic surface behavior. The primary focus of our previous study was on the fluid dynamical description of the newly found temporally transitional regime and the observed sporadic surface mobilization events. A diagnostic quantity termed mobilization index has been deduced that measures the stability of the temporarily stagnant surface and thereby allows for a prediction of further events of surface mobilization based on the current system behavior. The difference of the newly found behavior to the previously known stagnant lid and, particularly, to the episodic behavior has been documented by means of a Nusselt number–Rayleigh number scaling relationship. Of the different convective regimes, the temporally transitional behavior described by *Loddoch et al.* [2006] is of particular interest for the thermal evolution of terrestrial planets as it describes a scenario assumed to be relevant for Mars: although there is currently no evidence for recent or even ongoing plate tectonic activity on Mars [*Zuber*, 2001], some findings suggest the existence of an episode of active plate tectonics for early Mars. *Sleep* [1994] investigated the Martian crustal dichotomy [*Tanaka et al.*, 1992; *Smith et al.*, 1998] and, particularly, the northern lowlands with respect to a possible plate tectonic origin. He identified remnants of tectonic structures such as trenches, ridges, and transform faults and reconstructed a probable plate geometry, which is thought to have produced the dichotomy as it is observed today. A second set of indications that favors plate tectonics being active at some point in the Martian history results from the observations of the magnetometer and electron reflectometer (MAG/ER) experiment on board the Mars Global Surveyor spacecraft [*Acuña et al.*, 1992]. These measurements revealed that while Mars does currently not possess an actively generated magnetic field, the Martian crust is strongly magnetized with a magnitude more then ten times higher than that observed on Earth [*Connerney et al.*, 1999]. It has been suggested [*Stevenson*, 2001; *Connerney et al.*, 2005] that the recorded magnetic signatures have indeed been produced by a (reversing) core dynamo process during the early Martian history. That being the case, their linear shape and orientation mostly parallel to the dichotomy boundary fosters the conclusion that plate tectonics has been active during the operation of that Martian dynamo. Neither of the described observations provides compelling evidence for the presence of plate tectonics on Mars. Nevertheless, the elevated surface heat flux associated with a hypothetical early plate tectonics episode will have a major impact on the subsequent evolution of the planet and has, therefore, been considered in thermal evolution studies of Mars [*Nimmo and Stevenson*, 2000; *Breuer and Spohn*, 2003, 2006]. So far, thermal evolution studies incorporating a transition in the convective style have been conducted on the basis of parameterized convection models. These models do not consider the actual fluid dynamical system but parameterize the heat transport properties of mantle convection by more or less appropriate scaling laws. As a result, a change in the convective style has to be introduced artificially as discussed, for example, by *Nimmo and Stevenson* [2000] or *Breuer and Spohn* [2003].

[4] The present study follows a different approach by considering the full set of fluid dynamical equations (compare section 2.1). This method results in a computational burden significantly higher than that for parameterized convection models, discouraging its rigorous application in investigations that can be carried out using other techniques. With the increased capability of present-day computer systems and the exploitation of parallel computing techniques, this enterprise, however, becomes feasible. A drawback of the fluid dynamical model applied here is that some processes potentially relevant for the thermal evolution of a planet such as formation of new crust through partial melting cannot be accounted for. On the other hand, by following the described approach, a self-consistent investigation of temporal transitions in the convective style is possible as documented by *Loddoch et al.* [2006]. Furthermore, using a 3-D fluid dynamical model, the temperature distribution and the flow field within the model domain (i.e., the planetary mantle) are spatially resolved. In this paper, we therefore propose the application of a fluid dynamical model to investigate temporal variations in the convective style of planetary mantles and their influence on the thermal evolution of the respective planet, particularly that of Mars.

[5] As an example for the investigated temporal variability, Figure 1 presents a series of snapshots of the temperature field as observed for a model run that exhibits a short burst of plate tectonic activity followed by a longer period of stagnant lid convection [cf. *Loddoch et al.*, 2006]. At the beginning of the calculation the system exhibits quasi-stable stagnant lid convection. After 430 Ma the surface is partially mobilized at the front corner of the box and starts to move along the left boundary of the domain. Subduction of the surface material occurs in an elongated, slab-like structure perpendicular to the left side of the domain which propagates along with the movement of the surface. The convective pattern is now dominated by a large-scale flow corresponding to the flux of surface material. The surface mobility ceases after ~100 Ma and the stagnant layer (blue colors) is rebuilt. The negative temperature anomaly directly above the core-mantle boundary (CMB) caused by cold subducted material subsequently vanishes, and convection returns to a smaller scale, now being dominated by cold downwellings due to the internal heat generation [*Travis et al.*, 1990; *Weinstein and Olson*, 1990]. The situation depicted by Figure 1 is investigated in more detail later in this paper (section 3.3).

[6] This paper presents model calculations using a numerical mantle convection model (sections 2.1 and 2.2) that have been carried out for parameter values resulting in the temporally transitional behavior documented by *Loddoch et al.* [2006]. It is found that the observed sporadic surface mobilizations occur on time scales potentially relevant for a terrestrial planet. By an additional inclusion of an internal
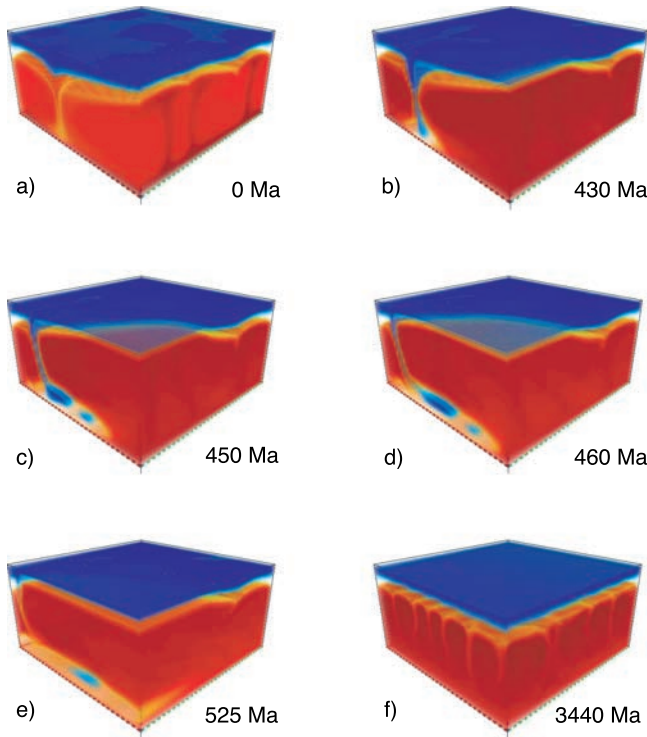
Figure 1. Visualization of the temperature field as observed during a sporadic event of surface mobilization as described by *Loddoch et al.* [2006]. Shown are snapshots of the color-coded temperature field taken at different times for a model run with internal heating and variable core temperature (compare section 3.3). Blue colors indicate cold material, while hot regions are shown in red. Mobilization of the surface is limited to about one third of the total surface area, roughly corresponding to the scenario proposed by *Sleep* [1994] for early Mars. Note that the mobilization is not triggered or terminated artificially but occurs self-consistently.

heat generation (section 2.3) and a variable core temperature (section 2.4) the results are interpreted in terms of their potential influence on the thermal history, including an early plate tectonics episode. A comparison with previously conducted thermal evolution studies is made in section 4.

[7] Our intention is not to present a comprehensive model of the thermal evolution of Mars but rather to transfer the insights that can be obtained only by means of fluid dynamical models to thermal history studies of Mars. The aim of this study is to investigate whether a change in the convective style and its consequences can be described by means of parameterized convection models.

2. Model

[8] For this study the numerical model initially presented by *Trompert and Hansen* [1998a] is applied. It has been used for a series of investigations of mantle convection with variable viscosity, including the successful, self-consistent generation of plate-like features [*Stein et al.*, 2004]. Recently, the same model has been applied to document temporal variations of mantle convection and the existence

of a new, temporally transitional convective regime [*Loddoch et al.*, 2006]. This latter study is continued in the present paper by investigating the observed behavior in terms of the thermal evolution of terrestrial planets. For this purpose the model used by *Loddoch et al.* [2006] is extended to include the effects of internal heat generation and the secular cooling of the core. These extensions are described in this section along with a brief presentation of the original model.

2.1. Fluid Dynamical and Numerical Model

[9] Thermally driven convection of an incompressible Boussinesq medium with infinite Prandtl number is considered. The governing equations describing the conservation of mass, momentum, and energy, respectively, are as follows:

$$\nabla \cdot \mathbf{u} = 0 \tag{1}$$

$$-\nabla p + \nabla \sigma + Ra\, T\hat{z} = 0 \tag{2}$$

$$\frac{\partial T}{\partial t} + \nabla(\mathbf{u}T) - \nabla^2 T = Q. \tag{3}$$

[10] Here $\mathbf{u}$ is the velocity vector, p is the dynamic pressure (i.e., the pressure without the hydrostatic component), and σ is the stress tensor with $\sigma = \eta[(\nabla \mathbf{u}) + (\nabla \mathbf{u})^t]$. T is the temperature, and $\hat{z}$ is the vertical unit vector. A temporally varying rate of internal heat production $Q(t)$ is introduced in section 2.3. The distribution of heat producing elements is assumed to be homogeneous, Q is hence spatially constant. All variables in equations (1)–(3) have been nondimensionalized using a common scaling based on thermal diffusion time and vertical temperature difference. The Rayleigh number resulting from this scaling (defined at the surface) reads

$$Ra = \frac{\alpha \rho g \Delta T d^3}{\kappa \eta_0}, \tag{4}$$

where α denotes the (constant) thermal expansivity, ρ denotes the density, g denotes the gravitational acceleration, ΔT denotes the vertical temperature difference, d denotes the height of the model volume, and κ denotes the (constant) coefficient of thermal diffusivity. The reference viscosity η_0 is defined at the surface of the box. Similar to the Rayleigh number given by equation (4), a modified Rayleigh number Ra_H expressing the amount of internal heating can be defined as

$$Ra_H = \frac{\alpha \rho g Q_0^* d^5}{\kappa \eta_0 k}, \tag{5}$$

where Q_0^* is the dimensional value of the initial heating rate and k denotes the thermal conductivity. Using Ra and Ra_H, the nondimensional heat production rate Q appearing in equation (3) can alternatively be expressed as follows, separated into a constant and a time-dependent part:

$$Q(t) = \frac{Ra_H}{Ra} Q'(t), \tag{6}$$

where $Q'(t)$ constitutes the time dependence decreasing exponentially from an initial value of unity.

[11] Equations (1)–(3) are solved using a numerical method presented by *Trompert and Hansen* [1996]: A finite volume approach is applied for spatial discretization and an implicit Crank-Nicholson scheme is applied for discretization in the time domain. The algebraic equations are solved iteratively, employing a multigrid technique with SIMPLER as smoother [*Patankar*, 1980]. The experiments were carried out in a Cartesian box with stress-free, impermeable boundaries. The box was cooled from above with constant temperature $T_{\text{top}} = 0$ (corresponding to a dimensional surface temperature of 200 K). The basal temperature is assumed to be spatially constant. Most of the calculations have been carried out with a variable core temperature according to section 2.4, only for the reference model a fixed core temperature of $T_{\text{bot}} = 1$, i.e., 1950 K was used. Reflecting conditions were employed at the sides. Here and later in this paper we scale our nondimensional quantities using values that have been reported to be representative for Mars [*Nimmo and Stevenson*, 2000] to obtain dimensional numbers.

2.2. Rheological Model

[12] The key ingredient for a fluid dynamical investigation of planetary mantle convection is a variable viscosity. For the mantle material of terrestrial planets the viscosity is found to depend on pressure, water content, strain rate, and most dominantly on temperature [*Karato et al.*, 1986; *Ranalli*, 1987; *Karato and Wu*, 1993]. Earlier studies [*Moresi and Solomatov*, 1998; *Tackley*, 2000a; *Stein et al.*, 2004] have shown that a viscosity depending on temperature and strain rate is sufficient to produce the three different and well-known styles of convection (see section 1). *Loddoch et al.* [2006] have shown that for critical parameter values a further, temporally transitional regime exists, which is to be explored in more detail in the present study. For this purpose we employ the same rheology previously used by *Stein et al.* [2004] and *Loddoch et al.* [2006]. The viscosity is assumed to depend on temperature T and effective strain rate E, which is defined as the second invariant of the strain rate tensor. The resulting viscosity $\eta(T, E)$ is calculated as follows:

$$\eta(T,E) = 2 \left[\frac{1}{\eta_T} + \frac{1}{\eta_E} \right]^{-1} \quad (7)$$

with

$$\eta_T = \exp(-rT) \quad \text{and} \quad \eta_E = \tilde{\eta} + \frac{\sigma_y}{E} \quad (8)$$

being the temperature-dependent and strain rate–dependent part of the viscosity, respectively. The strength of the temperature dependence is specified by r, with $R = \exp(r)$ being the viscosity contrast between the material with maximum (i.e., $T = 1$) and minimum temperature ($T = 0$). A lower limit for the strain rate–dependent part as required for numerical reasons is provided by the plastic viscosity $\tilde{\eta} = 10^{-5}$. The yield stress parameter σ_y controls the strain rate dependence of the overall viscosity with E being the effective strain rate as defined in section 2.2.

[13] *Stein et al.* [2004] have shown that the style of convection actually observed depends on the choice of parameters like the yield stress σ_y, the viscosity contrast R, as well as on the Rayleigh numbers Ra and Ra_H. The aim of our present study is not the systematic investigation of convective styles but rather the quantitative investigation and interpretation of the temporally transitional behavior found by *Loddoch et al.* [2006]. We therefore restrict the considered parameter range to fixed values of $\sigma_y = 10.0$ and $R = 10^5$ in the present study, i.e., to values for which the corresponding behavior is observed. For the parameters used later in this study ($Ra = 450$, d, κ etc. according to [*Nimmo and Stevenson*, 2000]) a scaling constant for the yield stress of $\sigma_{\text{ref}} \approx 4$ MPa is obtained, resulting in a dimensional yield stress of about 40 MPa. This value is in accordance with estimates for terrestrial planets [*Wuming et al.*, 1992; *Steinberger et al.*, 2001; *Lithgow-Bertelloni and Guynn*, 2004; *Fowler and O'Brien*, 2003]. A viscosity contrast of 10^5 corresponds to activation energies lower than typically considered for Mars. However, our investigations show that for a combined temperature dependence and strain rate dependence of the viscosity, a lower viscosity contrast (i.e., activation energy) is sufficient to correctly describe the fluid dynamics of mantle convection. An increased viscosity contrast would lead to a drastic increase of the temperature-dominated viscosity within the cold lid (for a fixed internal viscosity). As this region is already immobile, a further increase in the viscosity would have no qualitative effect on the dynamics of the system. The surface of a system in the stagnant lid regime would, therefore, remain stagnant. For systems that show mobile lid convection the overall viscosity is controlled by the strain rate–dependent part. An increased temperature dependence would only amplify this contribution because of the reciprocal summation in equation (7). While the rheology employed in our model remains an approximation of the actual rheology, it allows for a correct description of the fluid dynamical behavior of the system, which is the focus of our study.

2.3. Internal Heat Generation

[14] One assumption made in the model as used by *Loddoch et al.* [2006] is the neglect of an internal heating of the mantle caused by the decay of radioactive elements. This assumption is employed in many fluid dynamical investigations of mantle convection [e.g., *Solomatov and Moresi*, 1997; *Reese et al.*, 1998; *Moresi and Solomatov*, 1998]. However, radiogenic heating contributes substantially to the overall heat budget of a terrestrial planet and hence to its thermal evolution [*Schubert et al.*, 2001]. Therefore, a time-dependent internal heating rate is added in the present study, mimicking the decay of heat producing elements in the mantle.

[15] Typically, four different isotopes are considered for the production of heat within the mantle of terrestrial planets on geologic time scales: ^{40}K, ^{232}Th, ^{235}U, and ^{238}U [*Schubert et al.*, 2001]. The individual half-lives, specific heat production rates of these isotopes, and their present-day concentration relative to the parent element are documented and can be found in the literature [e.g., *Schubert et al.*, 2001]. Apart from these well-known physical properties the total amount of heat produced depends mainly on the abundance of the individual parent
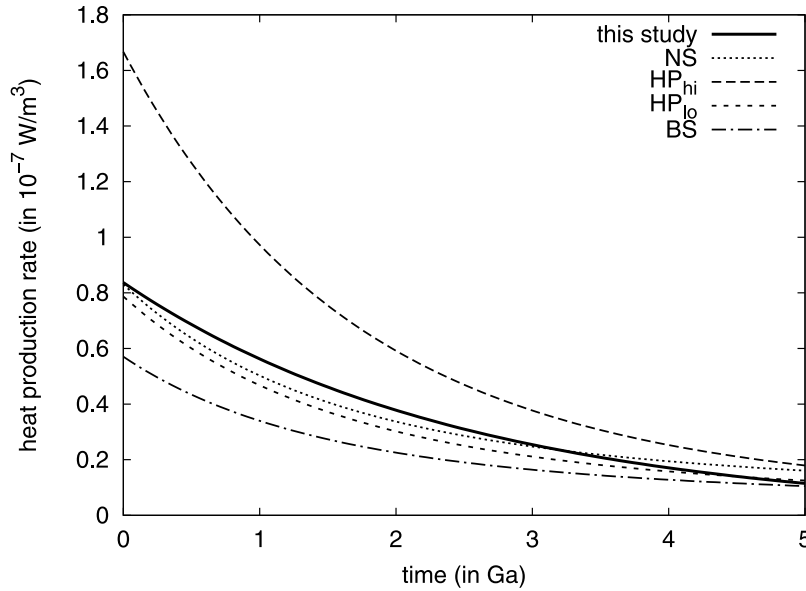
Figure 2. Comparison of the heat production rates as used in the thermal evolution studies by *Nimmo and Stevenson* [2000] (NS), *Hauck and Phillips* [2002] (HP), and *Breuer and Spohn* [2003] (BS). Additionally shown is a simplified, one-component heat production model as used in this study (solid black line).

elements, which may vary significantly among different types of rock. For nonterrestrial mantle rocks the composition cannot be determined directly and is, therefore, only poorly constrained [*Wänke and Dreibus*, 1994; *Lodders and Fegley*, 1997]. Figure 2 visualizes the heat production rates for several compositional models assumed to be representative for the Martian mantle. These models have been taken from different publications presenting thermal evolution models.

[16] However, the differences especially between the abundances employed by *Nimmo and Stevenson* [2000], *Hauck and Phillips* [2002], and *Breuer and Spohn* [2003] are relatively small. Because of the uncertainty of the exact composition, a simplified one-component internal heating model has been used in this study. The more complex four-component decay characteristics are approximated by a single exponential function:

$$Q^*(t) = Q_0^* \exp(-\lambda t). \tag{9}$$

Here the superscripted asterisk is introduced to indicate the dimensional heating rate as opposed to the nondimensional quantities appearing in the previous sections (compare equation (5)). By choosing the two parameters Q_0^* and λ accordingly, the heat production rates described by the compositional models mentioned above are approximated as

$$Q_0^* = 8.3 \times 10^{-8} \text{ W m}^{-3} \quad \text{and} \quad \lambda = 3.97 \times 10^{-10} \text{ a}^{-1} \tag{10}$$

For these values a nondimensional heating rate (equation (6)) of $Ra_H/Ra \approx 60$ is obtained. The temporal evolution of the heat production rate resulting from this simplified model is shown in Figure 2 as a solid black line.

2.4. Cooling Core

[17] The original model of *Trompert and Hansen* [1996] employs a temporally fixed basal temperature corresponding to a core that acts as an infinite heat reservoir for the overlying mantle. This simplification is reasonable for fluid dynamical investigations and has consequently been employed in the studies carried out by *Trompert and Hansen* [1998a] and *Stein et al.* [2004] using the same model or similar investigations by various other authors [e.g., *Moresi and Solomatov*, 1995; *Reese et al.*, 1998; *Moresi and Solomatov*, 1998; *Tackley*, 2000a, 2000b]. However, for an investigation of the thermal evolution of a planetary body the assumption of a fixed core temperature is too limiting. Here the secular cooling of the planet and hence a thermal coupling of the core and mantle have to be taken into account.

[18] Terrestrial planets like Mars, Venus, and Mercury are believed to possess a metallic core that is at least partially liquid [*Spohn*, 1991; *Stevenson et al.*, 1983]. Because of the much lower viscosity of liquid iron compared to that of mantle silicates, convection in the outer core can be assumed to be significantly more vigorous than in the mantle. The core is therefore considered to act as an isothermal heat reservoir for the overlying mantle where lateral temperature differences can be neglected, at least on mantle convection time scales [*Olson*, 2003]. As stated before, this heat reservoir is obviously not infinite. The heat that is removed from the core by conduction across the CMB causes the core to cool. The fluid dynamical representation of this mechanism is a core temperature that is not constant but rather varies according to the CMB heat flux. The total heat flow through the core-mantle boundary Φ_{cmb} into the mantle equals a loss of heat per unit time $\dot{Q}_c$ within the core:

$$\dot{Q}_c = \Phi_{cmb} \tag{11}$$

$$\Rightarrow \quad c_{p_c} m_c \frac{\partial T_c}{\partial t} = -A_m k \Delta T_{cmb}. \tag{12}$$

spherical　　　cartesian
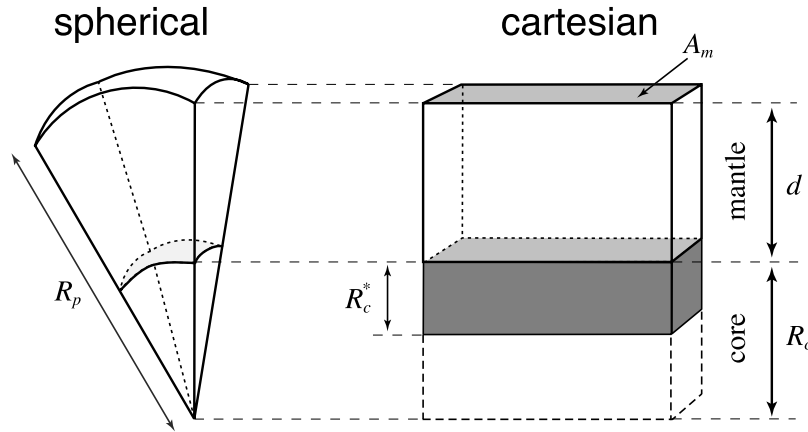
Figure 3. Comparison of the true, spherical geometry and the cartesian geometry as used in this study. The cartesian representation leads to an overestimation of the core size; therefore, a geometrically corrected core mass/size is used.

Discretizing the temporal derivative and solving for the core temperature of the new time step T_c^{n+1} yields

$$T_c^{n+1} = T_c^n - \frac{1}{c_{p_c} m_c} A_m k \Delta T_{\mathrm{cmb}}^n \Delta t, \tag{13}$$

where c_{pc} denotes the specific heat capacity of the core, m_c denotes the core mass, and T_c^{n+1} and T_c^n denote the core temperatures at time steps $n + 1$ and n, respectively with Δt being the corresponding time step size. A_m is the surface area of the core-mantle boundary, k is the thermal conductivity of the mantle material, and $\Delta T_{\mathrm{cmb}}^n$ is the temperature gradient across the CMB (considered at time step n).

[19] The mantle convection model used in this study is based on a Cartesian geometry. A direct extension of this geometry to the core leads to a cuboid shaped "pseudo-core" with a substantially overestimated core size if realistic values for mantle and core heights are applied. See Figure 3 for a visualization of the situation. Therefore, the core mass appearing in equation (13) is corrected for this geometrical effect, ensuring a correct volume ratio. For a spherical shell the core-mantle volume ratio, referred to as r_V, is given by the radii of core (R_c) and planet (R_p):

$$r_V := \frac{V_c^\circ}{V_m^\circ} = \frac{R_c^3}{R_p^3 - R_c^3}. \tag{14}$$

The same ratio is enforced for the Cartesian geometry by adjusting the volume V_c^* of the Cartesian core accordingly. This yields the modified Cartesian core mass m_c^* based on the (Cartesian) mantle volume

$$m_c^* = \rho_c A_m d r_V \tag{15}$$

with the density of the core ρ_c. For Mars-like values of the planetary and core radius of 3400 and 1450 km, respectively [*Nimmo and Stevenson*, 2000], a core-mantle volume ratio of $r_V = 0.084$ is obtained. Substituting equation (15) for the

core mass in equation (13), results in the following update rule for the (dimensional) core temperature:

$$T_c^{n+1} = T_c^n - \frac{1}{r_V} \frac{c_p \rho}{c_{p_c} \rho_c} \frac{\kappa}{d} \Delta T_{\mathrm{cmb}}^n \Delta t. \tag{16}$$

It should be noted that even with a core mass correction as described in section 2.4, our model geometry remains an approximation of the true spherical shape of terrestrial planets. The exact values, for example, for the core heat fluxes observed in this study might differ from those obtained for a spherical geometry. This, however, does not affect the overall findings described in this work, in particular the presence and consequences of the observed transitional behavior.

2.5. Mobilization Index

[20] Using the model described above and for a viscosity depending on temperature and strain rate (compare section 2.2), *Loddoch et al.* [2006] reported the existence of a novel convective regime. This newly found temporally transitional regime differs from both the episodic and the stagnant lid regime [*Moresi and Solomatov*, 1998] and is characterized by sporadic events of surface mobilization occurring out of a thermally equilibrated system state. Between two subsequent events of surface mobilization the observed behavior is indistinguishable from stagnant lid convection, at least by means of commonly considered quantities like the Nusselt number or the temperature profile. *Loddoch et al.* [2006] introduced the mobilization index ϵ_M defined as the ratio of the horizontally averaged effective strain rate at the surface to the applied yield stress:

$$\epsilon_M = \frac{\langle E \rangle_h}{\sigma_y}\bigg|_{\mathrm{surface}} \tag{17}$$

Using the mobilization index in (17), it is possible to quantify the stability of the (temporarily) immobile surface and, therefore, to predict the occurrence of further mobilization events [*Loddoch et al.*, 2006]: sporadic surface

mobility is only observed for systems with a mobilization index larger than unity, i.e., for $\epsilon_M > 1$.

[21] Furthermore, the mobilization index ϵ_M can be used to systematically describe the temporal characteristics of the newly found transitional behavior, which is discussed in more detail in section 3.

3. Results

3.1. Observed Time Scales

[22] The temporal characteristics of the newly found temporally transitional behavior have been investigated qualitatively by *Loddoch et al.* [2006] and recently also quantitatively by *Loddoch* [2007]. It has been shown that the frequency and the duration of the events of surface mobilization vary systematically as a function of the mobilization index ϵ_M. Two quantities are used for this purpose: the average stagnant lid time per event t_{SL}, given by

$$t_{SL} := \frac{t_{end}}{N}, \qquad (18)$$

i.e., the time over which the system was observed divided by the number of events during this time and the average mobilization time t_{mob}, which is defined as the sum of all (discrete) time step sizes Δt_i for which the system is in a mobilized state divided by the number of events N:

$$t_{mob} := \frac{1}{N} \sum_i \Delta t_i \quad \forall\, i\, :\, \epsilon_M\,(t_i) > th \qquad (19)$$

The system is considered being mobilized if the actual value of the mobilization index $\epsilon_M(t_i)$ exceeds a defined threshold th. A value of two times the average mobilization index of that model run has proven to provide a robust criterion ($th = 2 \times \overline{\epsilon_M}$).

[23] For systems at the parameter boundary between temporally transitional and episodic behavior, nondimensional stagnant lid times of $t_{SL} \approx 10^{-1}$ and mobilization times of $t_{mob} \approx 10^{-3}$ are found (measured in thermal diffusion times). As an example, Figure 4 shows an excerpt of the temporal evolution of the mobilization index for a model run in the corresponding parameter range. A constant core temperature, a surface Rayleigh number of $Ra = 450$, and no internal heating ($Q = 0$) have been employed. For this model run an average stagnant lid time of $t_{SL} = 5.7 \times 10^{-2}$ and an average mobilization time of $t_{mob} = 2.7 \times 10^{-3}$ thermal diffusion times have been calculated. Using a mantle height of $d = 1950$ km and a thermal diffusivity of $\kappa = 8 \times 10^{-7}$ m^2 s^{-1} [*Nimmo and Stevenson*, 2000], the dimensionalization $t^* = td^2\kappa^{-1}$ yields a thermal diffusion time of 4.75×10^{18} s, i.e., dimensional values of 8.6 Ga and 0.4 Ga for the observed stagnant lid and mobilization times, respectively. This corresponds to the time scales suggested by *Nimmo and Stevenson* [2000] and *Breuer and Spohn* [2003] as being relevant for a hypothetical plate tectonics episode on early Mars. The setup considered here represents a simplified model and uses parameters that differ from those probably relevant for early Mars (e.g., viscosity contrast and internal heating). This difference in parameter values will certainly impact the observed results quantitatively, as an increased Rayleigh number will move the
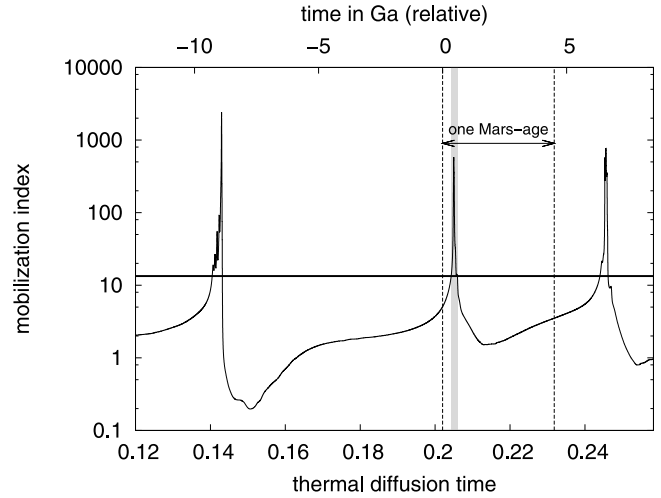

Figure 4. Mobilization index as a function of time for a model run that shows mobilization times relevant for Mars. Figure 4 shows an excerpt of the complete evolution. The grey area indicates a mobilized phase, according to the threshold introduced in equation (19).

system closer to the mobile lid regime and will thus lead to shorter time scales. An increase of the yield stress or of the viscosity contrast will have the opposite effect, as explored in detail by *Stein et al.* [2004]. However, the parameters chosen place the system in the convective regime that corresponds to the current fluid dynamical state of Mars, showing a stagnant lid–like behavior and allowing for sporadic events of surface mobilization. We are certain that as long as the system remains in the corresponding fluid dynamical regime, qualitative deviations from the actual parameter values (most of which are not known precisely anyway) are tolerable and do not influence the obtained results qualitatively. At the same time, the choice of parameters ensures that the problem remains computationally feasible, allowing for a fluid dynamical investigation of the system in three dimensions. Our intention at this point is not to present a comprehensive model of Martian mantle convection but to investigate the stagnation of a mobile surface from a fluid dynamical point of view. We therefore consider our model as a first approximation to the fluid dynamics that control the convective state of the mantle and thus the thermal evolution of the system. We will add effects of a cooling core and internal heat generation sections 3.2 and 3.3, respectively, thus moving the model setup closer to realistic conditions. A comparison with thermal evolution studies done in section 4 will show whether our simplified model can produce valid findings.

[24] The time span indicated in Figure 4 has been chosen such that the system shows an event of surface mobilization after ~350 Ma lasting for 260 Ma (grey area) followed by a period of vanishing surface mobility of >5 Ga. This behavior thus mimics the "early plate" situation on Mars proposed by *Nimmo and Stevenson* [2000]. In the following the influence of the observed intermittent plate tectonic activity on the subsequent thermal evolution of the system is investigated.

[25] A mobilization of the surface layer delivers large amounts of cold material to the convective interior and

a)

b)
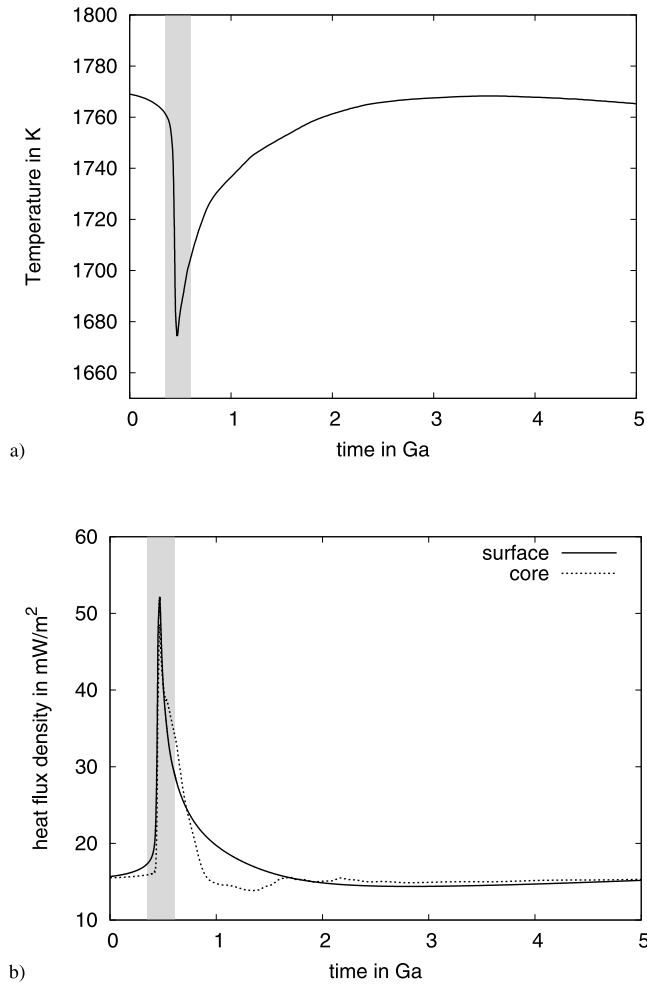
Figure 5. Temporal evolution of (a) the internal temperature and (b) the surface and basal heat fluxes for the scenario shown in Figure 4.

further to the base of the system, i.e., the core-mantle boundary. Consequently, the internal temperature of the system as well as the surface and basal heat fluxes vary significantly in response to the mobilization event as shown in Figure 5.

[26] The internal temperature, which is calculated as described in Appendix A, is 1770 K prior to the onset of mobilization. Once the mobilized cold surface material reaches the convective interior, the internal temperature drops almost instantly by 100 K. After the surface layer is rebuilt the internal temperature rises again, returning to its original value after 2.5 Ga. The subduction of cold material and its deposition at the core-mantle boundary are also reflected by the surface and basal heat fluxes which are calculated as follows:

$$q\big|_{\{top,base\}} := -k \frac{\partial \langle T \rangle_h}{\partial z}\bigg|_{z=\{d,0\}} \tag{20}$$

In this definition the advective heat flux is neglected because of the impermeable boundary conditions chosen. In the following a thermal conductivity of $k = 3.2$ W $(m\ K)^{-1}$

[Nimmo and Stevenson, 2000] and a temperature difference of $\Delta T = 1750$ K in addition to the mantle height of $d = 1950$ km already used above have been assumed. A surface temperature of $T_{surf} = 200$ K has been employed.

[27] The temporal evolution of the heat fluxes for the discussed model run is shown in Figure 5b. For both quantities the same initial value of 15 mW m^{-2} is observed, indicating a thermally equilibrated system. As the surface breaks apart, subducts, and is replaced by hot upwelling material, both heat fluxes increase significantly to a maximum value of 48.5 and 52.1 mW m^{-2} for the basal and surface value, respectively. While Figure 5b suggests that the increase of the heat fluxes occurs simultaneously, a closer inspection unveils a small time lag of 10 Ma. The delay in the rise of the basal heat flux corresponds to the time in which the subducting slab travels downward to the CMB. The velocity that corresponds to this time span is $v_{slab} = d/\Delta t \approx 20$ cm a^{-1}, a value that is confirmed by the maximum velocity observed during this phase.

3.2. Influence of a Cooling Core

[28] The results shown above have been obtained for a fixed basal, i.e., core temperature. As an extension to the model a thermal coupling of mantle and core as described in section 2.4 has been implemented and the calculation illustrated by Figure 5 has been repeated. The system state observed in the reference model (fixed core temperature) at $t = 0.202$ thermal diffusion times, i.e., $t = 0$ Ga in Figure 4, serves as initial condition. As the system state chosen results from a fluid dynamical calculation it implicitly fulfills the governing equations; that is, it represents a fluid dynamically valid state. An initial transient adjustment period caused by artificial initial conditions (such as a vanishing fluid velocity) is thus avoided. Additionally, because of the initial conditions chosen, an event of surface mobilization can be expected to occur during the time relevant for terrestrial planets.

[29] Qualitatively, the system behavior observed for a cooling core (shown in Figures 6a and 6b) is the same as that of the reference model with a fixed core temperature (Figure 5, note the different scales). After 480 Ma the surface is mobilized and subducted into the interior. Subsequently, the immobile surface layer is rebuilt, and the system returns to the stagnant lid–like mode of convection. However, since the system is not thermally buffered by a constant core temperature, the decrease in the internal mantle temperature is slightly stronger and permanent (Figure 6a, solid line). The mantle temperature does not return to the premobilization value but shows only a small increase followed by a monotonic and almost linear decline starting at 1 Ga, thus ∼500 Ma after the onset of the mobilization. At 4.5 Ga, i.e., after one planetary age, a final internal temperature of 1570 K is observed. As the core temperature is not fixed at the initial value in this model run, it varies according to the temperature of the overlying mantle. The temporal evolution of the core temperature (dotted line in Figure 6a) shows an initial decline, representing the disappearance of the bottom thermal boundary layer. Upon arrival of the cold subducted material at the core-mantle boundary (CMB) the core temperature drops from 1805 K by almost 200 K to a value of 1615 K. The core remains at this temperature for more than 1 Ga, after
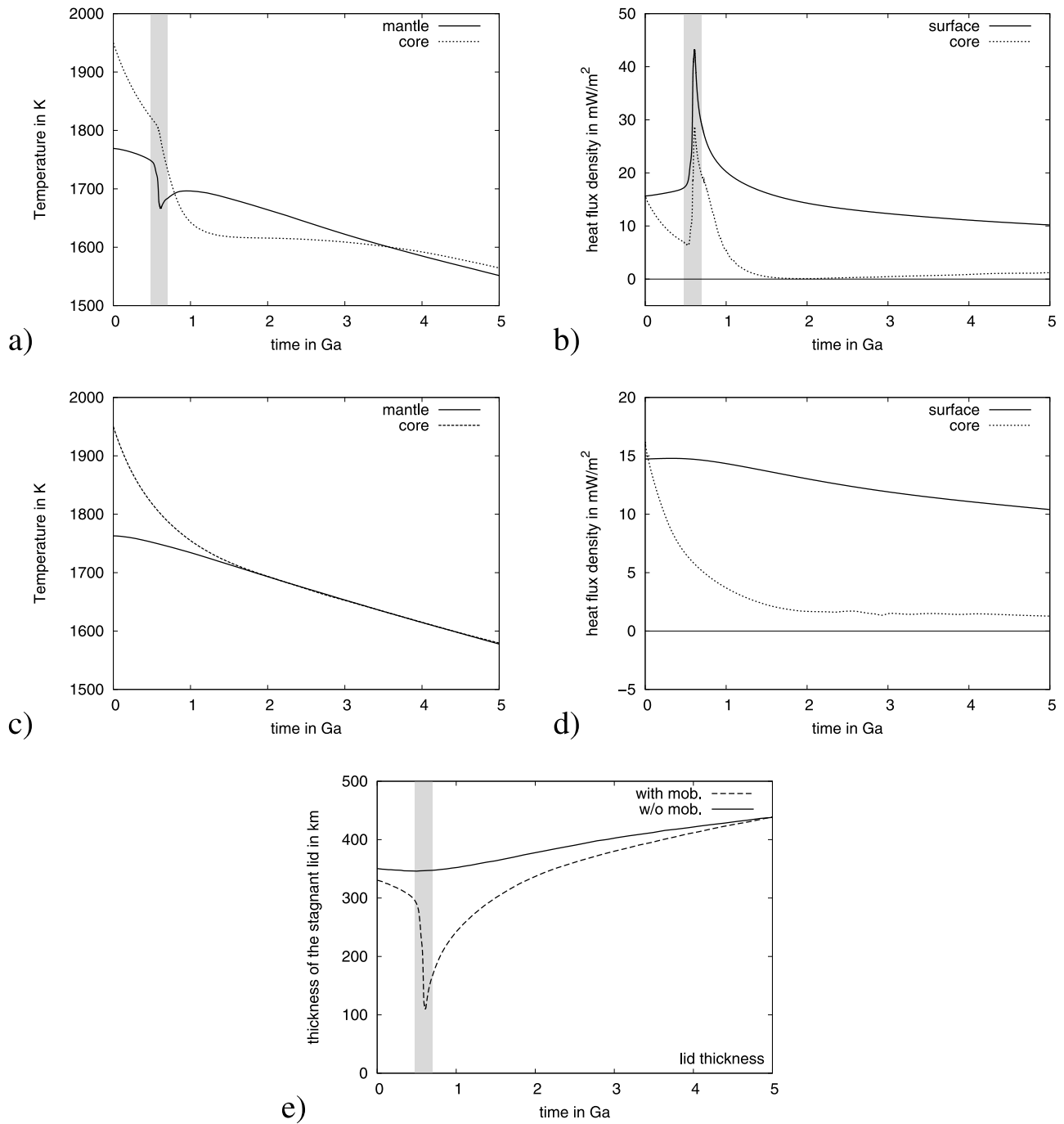
Figure 6. Thermal evolution of a system subject to secular cooling with and without a mobilization of the surface. The core and mantle temperature and the heat flux through the CMB and the surface are shown for systems (a and b) with and (c and d) without early mobilization events. (e) The thickness of the stagnant lid, calculated as described in Appendix A, is plotted as a function of time for both model runs. The grey vertical bar in Figures 6a, 6b, and 6e indicates the duration of the mobilization event according to the criterion given in equation (19).

which a further decrease to a final value of 1580 K at 4.5 Ga sets in. Figure 6a indicates that between $t = 0.8$ Ga and $t = 3.6$ Ga, the core temperature is lower than the mean internal temperature of the mantle. This corresponds to a transient inversion of the local temperature gradient caused by the subducted surface material locally reducing the temperature in the lower mantle.

[30] Figure 6b shows the temporal evolution of the surface and basal heat fluxes observed for the model run with surface mobilization and variable core temperature. The surface heat flux is nearly identical to that in the reference model with fixed core temperature (Figure 5b): a sharp increase is observed during the mobilization event (grey area) followed by a slower decrease. Differing from

the reference model, the heat flux does not return to its initial value of 15 mW m^{-2} but drops monotonically reaching 10.7 mW m^{-2} after 4.5 Ga. The core heat flux (dotted line in Figure 6b) shows an initial decrease owing to the reduction of the core-mantle temperature gradient already visible in the core temperature (Figure 6a). After the mobilization event and the peak-like increase the core heat flux drops to values close to zero since in this case not only the lower mantle but also the core is cooled by the cold slab. Note that the core heat flux remains positive throughout the time of observation despite the temperature inversion visible in Figure 6a. The "mantle temperature" as plotted in Figure 6a is the average internal temperature calculated as described in Appendix A. The temperatures observed in the lower mantle are indeed lower than this average value, resulting in a positive temperature gradient. However, directly above the core-mantle boundary the temperature gradient dT/dz is again negative, resulting in a positive core heat flux.

[31] In order to emphasize the influence of the mobilization event on the subsequent thermal evolution of the system, a second model run without a mobilization of the surface has been carried out. Again, the reference model with fixed core temperature presented in Figure 4 provides the initial conditions. Here the temperature, velocity, and pressure fields as observed at $t = 0.16$ thermal diffusion times have been used to start a calculation with variable core temperature. This choice provides maximum comparability between the two model runs (with and without mobilization) while ensuring that no mobilization of the surface occurs within the time span corresponding to one planetary age (compare Figure 4).

[32] The temporal evolution of the core and mantle temperatures observed in this case are plotted in Figure 6c. During the first 600 Ma the core temperature is virtually identical for the two model runs with and without mobilization (Figures 6a and 6c, dotted lines). Differing from the situation including a mobilization, the model without a mobilization of the surface does not show a spontaneous drop of the core temperature. Instead, the temperature declines rather slowly with time, reaching a value of $\sim T = 1600$ K after 4.5 Ga. This is only about 20 K more than observed in the model run with mobilization. In fact, the dramatic decrease of the core temperature following the mobilization event is compensated by a larger core cooling rate between 1.5 and 4.0 Ga. The internal temperature (solid line in Figure 6c) shows a similarly simple cooling behavior. After an initial adjustment period of ~ 300 Ma the internal temperature declines almost linearly with time, resulting in a temperature of $T_i = 1600$ K after 4.5 Ga. The same value is found for the core temperature at this time, representing a thermal equilibrium between core and mantle, at least in terms of the average internal temperature. In fact, the temperatures of the core and mantle are identical from 2 Ga onward, and the convective flow pattern is dominated by the cold downwelling plumes.

[33] The internal temperature T_i does not only provide information about the average temperature within the convective bulk of the mantle. As a byproduct the calculation of T_i as described in Appendix A additionally yields the thickness of the stagnant surface layer. This quantity is shown as a function of time in Figure 6e for the two model runs with and without a mobilization of the surface (dashed and solid lines, respectively). While the thickness of the stagnant lid is reduced significantly during the event of surface mobilization, it quickly returns to the initial value as the surface becomes immobile again. In fact, after 5 Ga the thickness of the lid is identical for the two model runs shown. If only the thickness of the stagnant lid is considered, which can be identified as the lithosphere [*Breuer and Spohn*, 2003], it may hence be impossible to distinguish between systems that have undergone an episode of active plate tectonics and those that maintained an immobile surface throughout time.

3.3. Internal Heat Generation

[34] In section 3.2 a thermal coupling between the mantle and a core with variable temperature has been introduced. Therewith, the influence of the observed spontaneous surface mobilization events on the thermal state of the core has been investigated. To provide further insights into the thermal evolution of terrestrial planets, an internal heating of the mantle due to the decay of radioactive isotopes is additionally taken into account.

[35] To investigate the combined effects of a secular cooling of the core, a potential mobilization of the surface and the presence of heat producing elements in the mantle, the model runs presented in section 3.2 have been repeated with an additional internal heating. Initial conditions identical to the one described in section 3.2 have been chosen. However, differing from the previous suite of runs, a value of $Ra_H = 9000$ for the internal heating Rayleigh number (equation (5)) has been employed. This results in a nonzero and exponentially decreasing source term in the heat transport equation (3) as described in section 2.3. In fact, the nondimensional heating rate at zero time resulting from this choice is $Q'(t = 0) = Ra_H/Ra = 20$, which is one third of the value elaborated in section 2.3 as being representative for Martian rock samples. This reduction reflects the fact that the mantle is depleted in heat producing elements because of crust formation. The depletion ratio of 1/3 used in the present investigation falls within the range of reasonable values according to the thermal evolution studies by *Breuer and Spohn* [2003]. The same depletion ratio has been used by *Harder and Christensen* [1996] for fluid dynamical studies of Martian mantle convection. The assumption of a temporally and spatially constant depletion ratio is, of course, only an approximation. It is, however, reasonable since the formation of new crust and hence the transfer of heat producing elements into the crust are neglected in the present model.

[36] The presence of internal heat production causes the mantle temperatures to be higher than those observed in the purely basally heated model runs presented in section 3.2, as is shown in Figure 7a. The mantle temperature T_i (solid line) increases by about 50 K during the first 400 Ma. As a result of the mobilization of the surface, T_i drops instantaneously by 60 K and subsequently increases again as the stagnant layer is rebuilt. A maximum temperature of 1920 K is reached at 2.4 Ga, after which the radiogenic heat production has decayed far enough and allows for a cooling of the mantle. After 4.5 Ga an average mantle temperature of 1880 K is observed, i.e., 110 K higher than the initial value. The core temperature (dotted line in Figure 7a) shows
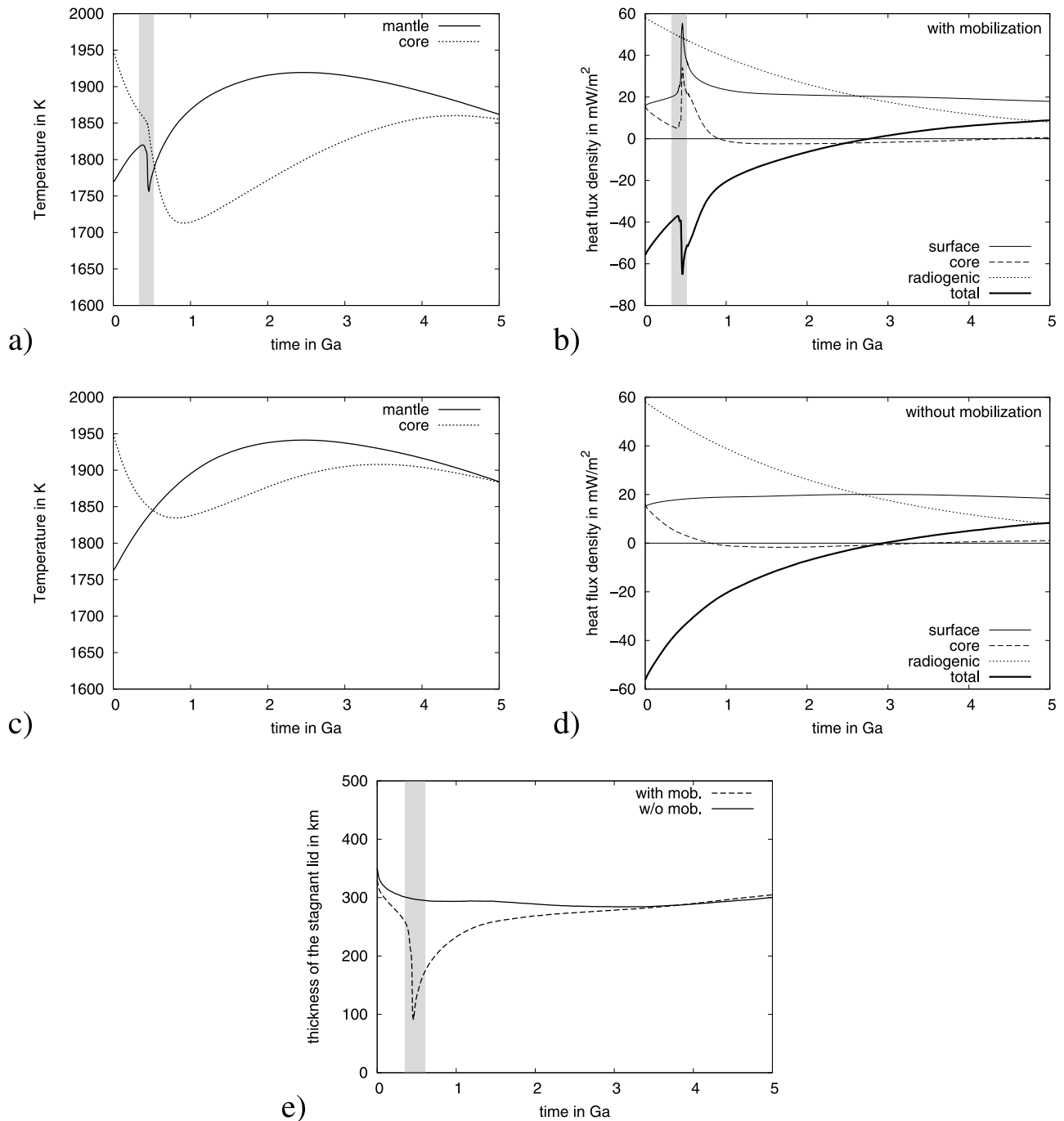
Figure 7. Core and mantle temperatures and heat flux for two models with internal heat generation (a and b) with and (c and d) without an early mobilization of the surface. (e) Thickness of the stagnant lid as calculated for the two model runs.

a temporal evolution similar to that presented in section 3.2 for systems without internal heating. In the present situation, however, the initial temperature decrease due to the disappearance of the (hot) bottom thermal boundary layer as well as the subsequent drop caused by the cold subducted surface material are less pronounced. The core temperature observed after the mobilization event is 1710 K, almost 100 K more than in the model runs without internal heating. Differing from the latter, the core is now heated by the hotter mantle, and the core temperature increases signifi-

cantly. At 4.5 Ga the maximum temperature of 1860 K is reached, equalling the premobilization value. Subsequent to the mobilization event, the core remains at a lower temperature than the overlying mantle throughout the observed time span. The temperature excess of the mantle relative to the core is largest after 1.25 Ga, where a temperature difference of 160 K is observed. Note that this difference is relative to the average internal temperature of the mantle calculated as described in Appendix A. The local temperature gradient across the core-mantle boundary is signifi-

cantly smaller and never exceeds a value of 25 K for this model run. After 4.5 Ga the temperature difference between mantle and core has declined to ∼20 K.

[37] The heating of the core by the mantle is also reflected by the respective heat fluxes which are plotted in Figure 7b as functions of time. The surface heat flux (q_{surf}, solid line) shows almost no variation after the typical perturbation caused by the mobilization event, similar to what is observed in the reference model (compare Figure 6). The core heat flux q_{core}, shown as a dashed line in Figure 7b, also resembles that observed for models without internal heating. However, because of the increased mantle temperature, the heat flux out of the core becomes negative between 1.0 and 4.4 Ga; that is, heat is transported conductively from the mantle into the core. Yet the overall variation of the core heat flux observed during this period is smaller than 5 mW m^{-2}. The large-scale increase of the total heat flux transported through of the system (thick solid line), which is calculated as $q_{total} := q_{surf} - q_{core} - q_h$, is mainly caused by the decline of the radiogenic heat flux q_h (dotted line).

[38] Corresponding to the investigation presented in section 3.2, the model run with internal heating was repeated for initial conditions that do not produce a mobilization of the stagnant surface layer. Figures 7c and 7d show the corresponding results for the core and mantle temperatures and the heat flux. Lacking a mobilization of the cold surface layer, the new model run does not show the characteristic drop of the core temperature at 450 Ma (dotted line in Figure 7c) observed for the model run with mobilization. Instead, the core temperature continues to decline smoothly reaching a (local) minimum after 800 Ma. At this point, the bottom thermal boundary layer has completely degraded because of the cooling of the core and the simultaneous increase of the mantle temperature caused by the internal heating. Subsequently, the mantle dominates the core temperature, which starts to increase again, similar to the model run with a mobilization of the surface. The maximum of 1910 K is reached after a total time of 3.5 Ga. Now the concentration of heat producing elements in the mantle is low enough to allow for an overall cooling of the system and the core temperature enters the final cooling stage. After 4.5 Ga a core temperature of 1895 K is observed, only 35 K more than in the model run with an early mobilization.

[39] The temporal evolution of the two mantle temperatures shown in Figures 7a and 7c bear the same similarities as already found in the two model runs with a purely basal heating (Figures 6a and 6c). After the drastic temperature drop occurring at 450 Ma the two lines plotted are virtually parallel with an offset of about 23 K. The final temperature after 4.5 Ga for the model run without an early mobilization is thus 1902 K compared to the 1880 K observed for the model run including a mobilization of the surface. The maximum mantle temperature observed in this model run is 1940 K (at 2.4 Ga). Figure 7e shows the thickness of the stagnant lid as a function of time for the two model runs with internal heat generation. Similar to the situation without internal heating, the model runs with and without a mobilization produce virtually identical lid thicknesses after 4.5 Ga. However, because of the presence of an internal heat generation and thus higher mantle temperatures (Figures 6a and 7a) and, simultaneously, a higher surface heat flux (compare Figures 6b and 7b), the absolute value of the lid
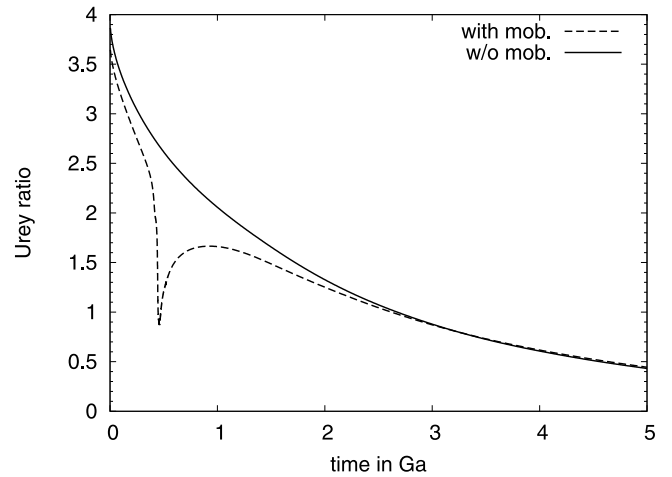
Figure 8. Temporal evolution of the Urey ratio Ur, i.e., the ratio of the radiogenic heat flux to the overall surface heat flux.

thickness observed after one planetary age is reduced by 135 km. The final value of 300 km is even lower than the initial lid thickness of 350 km. As already visible in the model runs without internal heating (Figure 6e) the thickness of the stagnant lid remains at values larger than zero, even during the mobilization event. This effect is caused by the surface being not completely mobilized. In this model run, only one third of the stagnant layer is affected by the mobilization, a situation corresponding roughly to the plate geometry proposed by *Sleep* [1994] to have caused the Martian crustal dichotomy. A partial mobilization of the stagnant surface as seen here can only be observed in a 3-D fluid dynamical model and cannot be accounted for in parameterized convection models. A series of snapshots of the temperature field as observed for this model run illustrating the mobilization event has been shown in Figure 1.

[40] As already seen in Figure 7 the internal heat production contributes significantly to the overall heat budget of the system. This contribution is measured by the Urey ratio, which relates the radiogenic heat flux q_h to the total heat flux through the surface of the system q_{surf} [*Schubert et al.*, 2001]:

$$Ur := \frac{q_h}{q_{surf}}. \tag{21}$$

Note that in the present case the Urey ratio can be calculated in terms of the heat flux, as a Cartesian model domain is considered. Figure 8 shows the Urey ratio as a function of time for the two model runs with internal heating presented in this section. For both model runs the initial value is significantly larger than unity; that is, more heat is generated by radioactive decay than is removed through the surface of the system. Consequently, the mantle temperature increases as shown in Figures 7a and 7c. As the rate of internal heat production decreases, the Urey ratio is likewise reduced. For both model runs, i.e., with and without a mobilization of the surface, an Urey ratio of $Ur = 1$ is reached at 2.7 Ga. After one planetary age, both model

runs yield a value of $Ur = 0.5$, indicating that for the considered model system, 50% of the present-day surface heat flux is due to radiogenic heating (as with the present-day Earth).

4. Comparison With Parameterized Convection Models

[41] In section 3 the influence of the newly discovered sporadic mobilization events on the subsequent thermal evolution of the convective system has been investigated. For this purpose a decaying abundance of heat producing elements and a variable basal temperature mimicking a core subject to secular cooling have been included in the model. The investigated scenario of an early event of surface mobilization followed by stagnant lid convection is potentially relevant for Mars [*Nimmo and Stevenson*, 2000; *Breuer and Spohn*, 2003]. In this section the obtained results are compared with previous investigations of the Martian thermal evolution. The main question here is whether a parameterized convection model using quasi steady state convection describes the transition from a mobile to a stagnant surface correctly.

[42] The studies carried out by *Nimmo and Stevenson* [2000], *Hauck and Phillips* [2002], and *Breuer and Spohn* [2003] reflect the state of the art in the investigation of Mars' thermal history. The applied models incorporate effects of secular cooling and internal heating as investigated in section 3. Furthermore, the generation of new crust by partial melting, its recycling through crustal delamination, and other processes that may influence the thermal evolution are taken into account. However, all three studies employ so-called parameterized convection models. Differing from the present study, these models do not solve the governing set of fluid dynamical equations presented in section 2 but consider only the thermodynamics of the convective system. The heat transport properties of thermal convection are expressed in terms of more or less appropriate scaling relationships. These scaling laws relate diagnostic quantities like the Nusselt number (i.e., the heat flux) or the average convective velocity to system parameters such as the amount of basal or internal heating or the viscosity contrast. The most common relation is the Nusselt number−Rayleigh number scaling

$$Nu = aRa^b \tag{22}$$

which has been the subject of a vast amount of analytical, numerical, as well as experimental investigations [e.g., *Booker*, 1976; *Roberts*, 1977; *Nataf and Richter*, 1982; *Solomatov*, 1995; *Trompert and Hansen*, 1998b; *Solomatov and Moresi*, 2000]. Depending on the boundary conditions, the mode of heating (basal/internal), and also the style of convection, different values for the two parameters a and b are found, in particular for the scaling exponent b.

[43] Once a relevant value for b (and a) is obtained, equations like (22) can be used to infer the thermal evolution of a planetary mantle as follows. The heat flux through the system for a given temperature difference (i.e., Rayleigh number) is calculated using equation (22). This heat flux out of the system corresponds to a change of the total amount of heat in the system and thus causes a

reduction of the temperature. The temperature reduction, in turn, results in a new value of the Rayleigh number which can then be used to repeat the described iterative process. In fact, current parameterized convection models such as that used by *Breuer and Spohn* [2003] employ techniques that are more sophisticated, but the principle is as demonstrated. The described scheme provides a computationally very efficient technique to investigate the thermal evolution of terrestrial planets like Mars. However, it cannot account for the spatial structure of the convection pattern (e.g., the temperature distribution) or for dynamical effects such as a sporadic mobilization of the surface. Finally, its applicability is constrained by the validity of the employed scaling relations and the chosen values for a and b. While *Choblet and Sotin* [2000] showed that the thermodynamics of a planetary mantle subject to secular cooling through a stagnant lid may indeed be described by a single quasi-static scaling law, this is certainly not the case for a system that undergoes a transition from one convective style to another. On the other hand, the model used in the present study neglects some processes potentially relevant for terrestrial planets, like partial melting and the formation of crustal material, because of its fluid dynamical origin. It can hence be argued that the applicability of the obtained results to actual planetary bodies is somewhat limited. Nevertheless, a correct description of dynamical processes such as mantle convection and plate tectonics is possible only by means of a full-fledged fluid dynamical model. Particularly, the cessation of plate tectonics cannot be investigated consistently by other means. *Nimmo and Stevenson* [2000] tried to work around this problem by implementing different scaling laws for the individual convective stages with a change in the governing relation at an arbitrary point in time. For the phase characterized by stagnant lid convection these authors used a constant $Nu − Ra$ scaling exponent of one third as resulting from boundary layer theory [cf. *Schubert et al.*, 2001]. However, for variable viscosity convection this value is not valid [e.g., *Christensen*, 1984; *Hansen and Yuen*, 1993]. For the calculations presented in section 3, for instance, i.e., a setup corresponding to that considered by *Nimmo and Stevenson* [2000], a scaling exponent of $b = 0.286$ has been found.

[44] Besides this rather general discrepancy between the present study and parameterized convection models, the study performed by *Nimmo and Stevenson* [2000] yields some results that cannot be confirmed by the present investigation. The most obvious feature is that their model shows a monotonic decline of the mantle temperature in the nonmobilized model run. There, no increase of the mantle temperature caused by the internal heating as clearly visible in Figure 7c is observed, although the assumed concentration of heat producing elements is even larger than in the present study. This contradiction is probably attributed to an overestimated surface heat flux caused by the large scaling exponent of one third for the $Nu − Ra$ relation, as discussed above. Figure 9 compares the surface heat flux as observed for the two model runs presented in section 3. The solid line indicates the model run without a mobilization of the surface, corresponding to the stagnant lid case investigated by *Nimmo and Stevenson* [2000] (therein, model "A"). The heat flux values observed here are in the range of $15 − 20$ mW m^{-2}, varying only marginally with time as
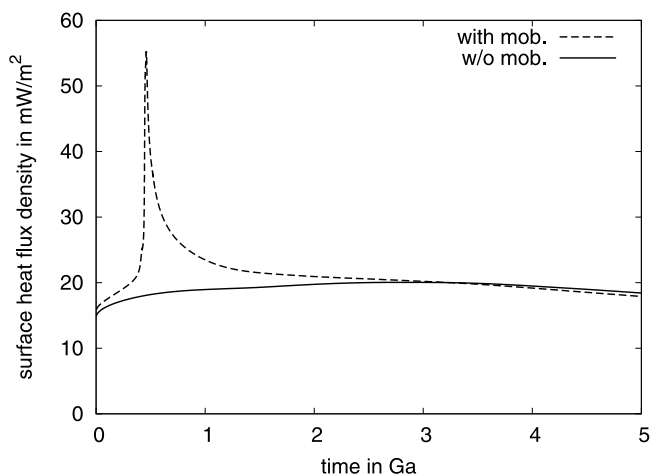
Figure 9. Temporal evolution of the surface heat flux for the two model runs with internal heating (compare section 3.3).

opposed to the results of *Nimmo and Stevenson* [2000], who find initial surface heat flux exceeding 100 mW m^{-2}. This difference might partially be attributed to the different initial conditions adopted. Another factor that contributes to this phenomenon is the lack of a spatially varying mantle temperature in their model, which leads to an immediate coupling of the temperature variations at the core and the surface. The fluid dynamical model used here allows the mantle to change its temperature locally in response to a change in the core heat flux. The temperature perturbation reaches the surface only after some time determined by the thermal conductivity of the material and the vigor of convection.

[45] A core with variable temperature as introduced in section 3 does not only serve as a thermal energy reservoir for the overlying mantle. The core of a terrestrial planet furthermore represents an individual fluid dynamical system: thermochemical convection in the ferrous core is responsible for the dynamic generation of the planet's magnetic field. Although these processes are out of the scope of the present study, the temporal variation of the basal heat flux potentially has a strong influence on the fluid dynamics of the core. *Nimmo and Stevenson* [2000] have investigated mantle thermodynamics and plate tectonics on Mars with respect to an active dynamo process in the Martian core. They estimated a maximum heat flux out of the core of $5-19$ mW m^{-2} that could be sustained by the core purely conductively, i.e., without the need for convective heat transport. Above this range, convection in the core sets in and the generation of a magnetic field would become possible. Figure 10 shows the core heat flux as calculated in the present study for the two model runs, incorporating an internal heating of the mantle. In addition to the two temporal evolutions of q_c, the critical core heat flux interval deduced by *Nimmo and Stevenson* [2000] is plotted, indicated by the grey area. The model run without an early mobilization of the surface (solid line) produces a core heat flux in the critical range only during the first 400 Ma of the initial cooling period. The model run that includes a surface mobilization event starts at the same initial core heat flux

value. However, after 400 Ma, the subducted cold surface material causes a rapid increase of the core heat flux that exceeds the upper limit of the conductive range of 19 mW m^{-2}. According to the estimate of *Nimmo and Stevenson* [2000], the core is likely to be convecting at least during the high heat flux stage lasting in this model for 120 Ma. A dynamo process producing a global magnetic field is, therefore, favorable for this stage, paralleling the conclusion of *Nimmo and Stevenson* [2000]. From 1 Ga onward, both model runs (with and without surface mobilization) show a negative core heat flux as visible in Figure 10. In this situation the temperature in the lower mantle increases because of the internal heating to values exceeding that of the core. Consequently, the core is heated by the mantle, and its temperature subsequently rises again. The strength and duration of this reversed core heat flux period depends mainly on the lower mantle temperature and on the vigor of convection, i.e., the efficiency of heat removal from the CMB. For the model run without a mobilization of the surface (solid line in Figure 10) the core heat flux returns to positive values at 3.5 Ga. The model that includes a mobilization sustains a negative core heat flux until 4.5 Ga (dashed line) caused by the deposition of cold surface material in the lower mantle. Because of the higher surface heat flux and hence a more efficient cooling of the mantle, the model of *Nimmo and Stevenson* [2000] exhibits this temporary inversion of the core heat flux only during the artificially introduced conductive stage following the termination of the plate tectonics episode, see below.

[46] A central element of the investigation of *Nimmo and Stevenson* [2000] is the influence of an early episode of plate tectonics on the subsequent thermal evolution. In order to do so within the limits of a parameterized convection model, the authors introduced a three-stage thermal history for Mars: Initially, the planet is assumed to show plate tectonics, resulting in a comparatively large surface heat flux in their model given by a constant viscosity convection scaling exponent. This high heat flux stage is terminated artificially after 500 Ma, and mobile lid convection is replaced by a purely conductive state, i.e., a situation in which the convective motion in the entire mantle is assumed to have vanished. After the top thermal boundary layer has grown to a critical thickness, convection sets in again, now being confined to the volume beneath the stagnant surface layer. In their model runs the purely conductive stage is found to last for 1.2 Ga. The fluid dynamical investigations presented here also show an adjustment period directly following the mobilization event. Considering the thickness of the stagnant lid (i.e., a similar quantity as used by *Nimmo and Stevenson* [2000] as a criterion), this period does indeed last for ~1 Ga, after which the premobilization value for the lid thickness is restored (compare Figure 7e). However, during this period the convective motion does not die off as assumed by *Nimmo and Stevenson* [2000]. Figure 11 shows the temporal evolution of the globally averaged root-mean-square velocity for the two model runs discussed in section 3. The mobilization of the surface is clearly visible as a peak-like increase in the average velocity for the corresponding model run (dashed line). While a reduction of the velocity is indeed exhibited as the stagnant surface is rebuilt, the value does not drop to zero and is only
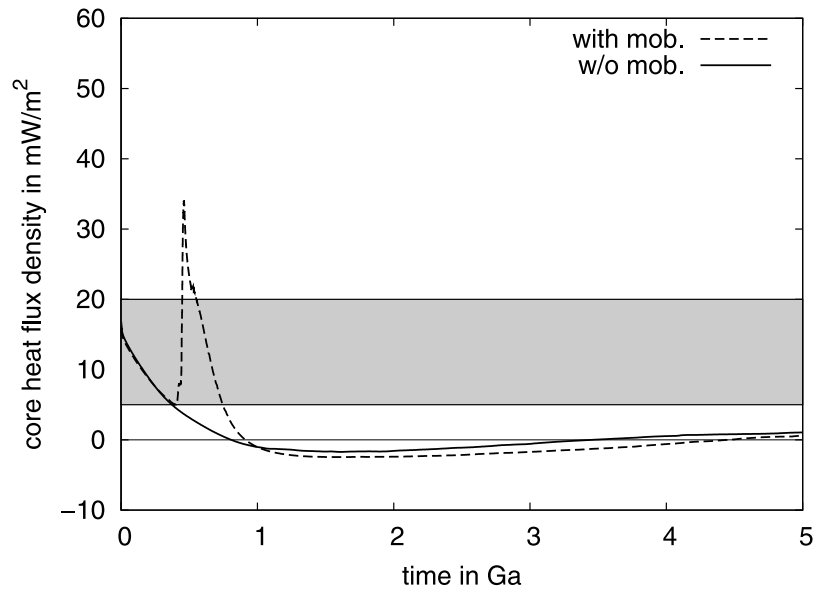
Figure 10. Heat flux out of the core as a function of time. Two model runs with and without a mobilization of the surface (dashed and solid lines, respectively) are shown. The grey area indicates the maximum conductive core heat flux according to *Nimmo and Stevenson* [2000].

marginally smaller than the value observed for the purely stagnant lid case (solid line). The assumption of a post-mobilization phase with vanishing convective motion therefore contradicts the findings of the fluid dynamical investigation presented here.

[47] The results of the present study are generally in accordance with the findings of the considered parameterized convection model. Because of the simplified assumptions made in the model of *Nimmo and Stevenson* [2000], some of their observations, however, contradict those made in the present fluid dynamical investigation.

[48] *Breuer and Spohn* [2003] also investigated the thermal evolution and studied the influence of an early episode of plate tectonics. Similar to the work of *Nimmo and*

Figure 11. Globally averaged root-mean-square velocity as a function of time. Two model runs with and without a mobilization of the surface (dashed and solid lines, respectively) are shown.

Stevenson [2000], *Breuer and Spohn* [2003] followed a parameterized convection approach. However, as they employed a more sophisticated model to describe the transition from mobile to stagnant surface, their results are found to be in better agreement with the fluid dynamical investigation presented in this study. *Breuer and Spohn* [2003] additionally included the effects of partial melting, crustal growth, and segregation of heat producing elements into the crust. As these processes have been neglected in the present work, a detailed quantitative comparison between the two studies is thought to be inappropriate.

5. Summary and Conclusion

[49] Temporal variations in the convective style and, consequently, in the surface behavior as observed by *Loddoch et al.* [2006] are naturally of major importance for the description and understanding of fluid dynamical systems in general. If the systems studied here are considered to be representative for the silicate mantles of terrestrial planets, the observed phenomena are likewise relevant for planetological considerations. The findings of our previous study [*Loddoch et al.*, 2006] have been found to be applicable to the evolution of planetary bodies in terms of the time scales observed (section 3.1). Accordingly, calculations have been presented here that reproduce the situation in terrestrial planets as closely as possible within the limits of the model used. The calculations carried out focus explicitly on the presence of an early era of surface mobility followed by stagnant lid convection extending to the end of one planetary age. While this scenario has been suggested and is incorporated in thermal evolution models of Mars [*Nimmo and Stevenson*, 2000; *Breuer and Spohn*, 2003, 2006], it has, until now, never been approached using fluid dynamical techniques. The fundamental question is, therefore, whether an endogenic
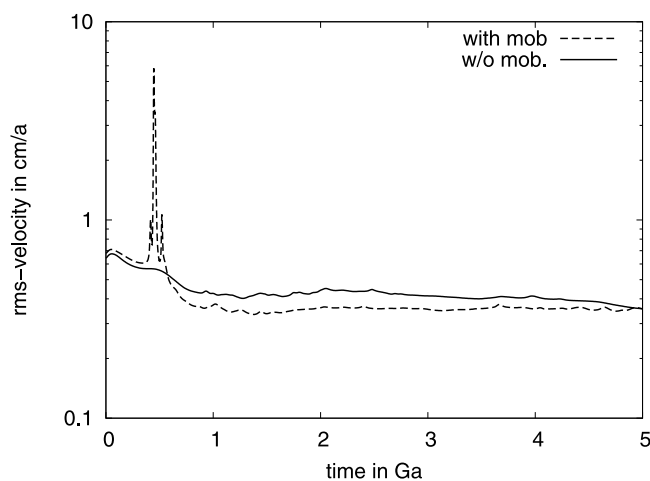
cessation of hypothesized plate tectonics is possible in the first place. Of similar importance are the so far unresolved questions of how this transition from mobile lid to stagnant lid convection proceeds and what the influence on the subsequent thermal evolution of the planet might be and whether it can be appropriately be described by parameterized convection models. This study has shown that intermittent changes in the surface behavior are an inherent feature of the dynamics of a convective system and may indeed occur on time scales relevant for terrestrial planets. For the first time the current model provides information about the temperature distribution and the flow field for the transition period from plate tectonics to stagnant lid convection, both temporally and spatially resolved. The obtained results are found in reasonable accordance with previously conducted investigations employing more simplified, thermodynamical models (specifically those of *Nimmo and Stevenson* [2000]). Our results, therefore, suggest that simplified models that do not account for the full fluid dynamics of mantle convection but are based on scaling relationships are indeed able to describe the thermal evolution of a planetary mantle correctly, even if the planet has undergone a change in the convective style. This is true at least if advanced models are employed to describe this transition as, for example, done by *Breuer and Spohn* [2003].

[50] Similar to earlier investigations, the influence of an early plate tectonics episode on the (thermo) dynamics of the core has been evaluated in the present study. Here the correlation between the exhibited surface behavior and the core's ability to sustain a dynamo generating a magnetic field is of interest. Again, the findings reflect those obtained using parameterized convection models: the presence of plate tectonics results in an elevated core heat flux well above the critical value necessary for the core to convect [*Nimmo and Stevenson*, 2000; *Breuer and Spohn*, 2003]. There is, however, one severe shortcoming in this mantle-based consideration. An excess of the critical core heat flux of $5-19$ mW m^{-2}, which can be transported out of the core purely conductively according to *Nimmo and Stevenson* [2000], is not a sufficient nor, in particular, a necessary criterion for the presence of core convection and the generation of a magnetic field. The described, rather simple conclusion is based on the assumption that convection in the core is purely thermally driven and necessarily supercritical. The presence of an additional, lighter constituent in the ferric core such as sulfur [*Stevenson et al.*, 1983; *Schubert and Spohn*, 1990] opens the possibility for core convection being driven compositionally [*Turner*, 1980], which may occur for subcritical thermal Rayleigh numbers as investigated by *Hansen and Yuen* [1989]. The work of *Stellmach and Hansen* [2004] revealed that for thermally driven convection in the presence of a magnetic field, core convection and a dynamo process are possible for parameters which would not allow for nonmagnetic convection (i.e., convection in the absence of a magnetic field) at all. The estimate on the generation of a Martian magnetic field in terms of the maximum conductive core heat flux as given by *Nimmo and Stevenson* [2000] and considered by several other studies may provide a first-order approximation of the relationship of mantle convection and magnetic field history. However, for a correct and comprehensive investigation of this important aspect of planetary evolution, further combined studies of the fluid dynamics of mantle and core are necessary.

Appendix A: Definition of an Internal Temperature

[51] In section 3 the internal temperature T_i has been used to characterize the thermal state of the investigated convective systems. How this quantity is defined and calculated is the subject of this appendix.

[52] Apart from the heat fluxes through the surface and the base, the temperature inside the model domain (i.e., the planetary mantle) is of interest for the description of the thermal state and evolution of the investigated system. Here the temperature of the convective interior (or internal temperature) is of particular importance since this value controls the (temperature-dependent) viscosity and has hence a strong influence on the dynamics of the convective system. This quantity is not directly available as, for example, the globally averaged temperature or the temperature at a specific depth but has to be calculated. In order to obtain the internal temperature, the "convective interior" (i.e., the region for which the temperature is sought) has to be defined. Figure A1 shows a temperature profile typically observed for stagnant lid convection. The topmost part of the profile (here $z \geq 0.81$) is characterized by a nearly linear increase of temperature with depth. This region corresponds to the immobile stagnant lid, in which heat is transported only by conduction, resulting in a constant heat flux q_{top} (i.e., a linear temperature profile). Below the stagnant lid the system and, consequently, the temperature profile are dominated by convective motion: the bulk of this region is almost isothermal, and thin thermal boundary layers (TBL) develop at the upper and lower border, i.e., directly below the stagnant lid and above the hot base of the system. As the material below the stagnant lid can effectively be considered as being isoviscous, the temperature profile within this part of the system is virtually symmetric [*Turcotte and Schubert*, 2002]. Consequently, the internal temperature is identical to the average temperature of the convective bulk (white area in Figure A1).

[53] The following scheme is applied to calculate the thickness of the stagnant lid and, therewith, the internal temperature (note that all appearing quantities are nondimensional).
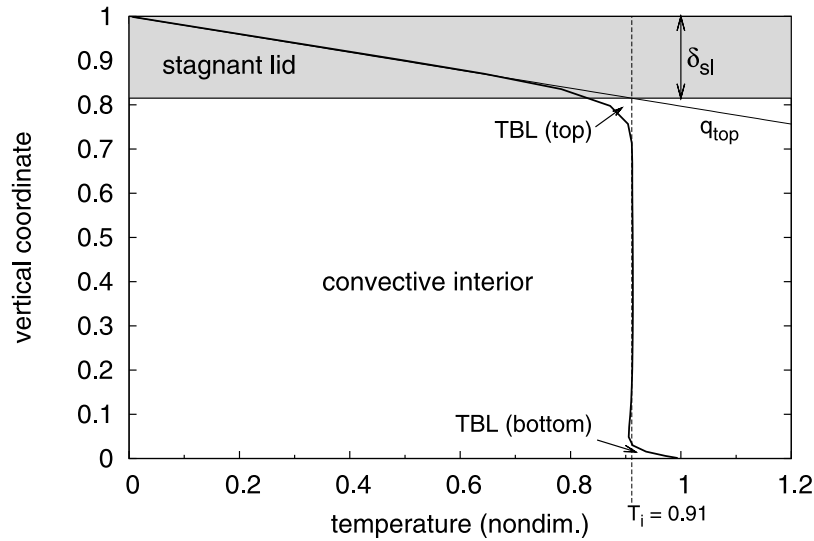
[54] 1. The horizontally averaged temperature of the topmost layer $\langle T(z_{NZ}) \rangle_h$ is used together with the surface temperature $T_{\text{surf}} = 0$ to calculate the surface heat flux

$$q_{\text{top}} = -\frac{T_{\text{surf}} - \langle T(z_{NZ}) \rangle_h}{1 - z_{NZ}},$$

where z_{NZ} denotes the vertical coordinate of the topmost layer.

[55] 2. The horizontally averaged temperature in the middle of the box is used as an approximate value for the internal temperature

$$T_i^* := \langle T(z = 0.5) \rangle_h$$

Figure A1. Horizontally averaged temperature T as a function of the vertical coordinate z as typically obtained for stagnant lid convection (here for $Ra = 450$ and $\sigma_y = 10.0$). Figure A1 illustrates the location of the lower boundary of the stagnant lid at the intersection point of surface temperature gradient q_{top} and internal temperature T_i.

[56] 3. The surface heat flux q_{top} and the approximate internal temperature are used to calculate the (approximate) thickness of the stagnant lid as

$$\delta_{sl}^* := -\frac{T_i^*}{q_{top}}.$$

Graphically, this corresponds to the depth at which the linear surface temperature gradient intersects the internal temperature.

[57] 4. The internal temperature is now calculated as the horizontally and vertically averaged temperature below the stagnant lid:

$$T_i := \frac{1}{1 - \delta_{sl}^*} \int_0^{1-\delta_{sl}^*} \langle T(z) \rangle_h \, dz.$$

[58] 5. The new internal temperature is then used to update the thickness of the stagnant lid according to step 3:

$$\delta_{sl} := -\frac{T_i}{q_{top}}.$$

[59] While the last two steps of this scheme could be applied repeatedly, tests have shown that a further iteration does not yield significantly different results.

[60] Within the course of this study, the described definition of the interior temperature has proven to be suitable and robust and does provide reasonable values, even during an event of surface mobilization. *Moresi and Solomatov* [1995] suggested a similar iterative technique to calculate the temperature of the isothermal interior. Their definition, however, considers the stagnant lid and the top thermal boundary as a single combined layer. Consequently, *Moresi*

and Solomatov [1995] are unable to calculate values for the thickness of the stagnant lid individually.

References

Acuña, M. H., et al. (1992), Mars Observer magnetic fields investigation, *J. Geophys. Res.*, *97*, 7799–7814.

Booker, J. (1976), Thermal convection with strongly temperature-dependent viscosity, *J. Fluid Mech.*, *76*, 741–754.

Breuer, D., and T. Spohn (2003), Early plate tectonics versus single-plate tectonics on Mars: Evidence from magnetic field history and crust evolution, *J. Geophys. Res.*, *108*(E7), 5072, doi:10.1029/2002JE001999.

Breuer, D., and T. Spohn (2006), Viscosity of the Martian mantle and its initial temperature: Constraints from crust formation history and the evolution of the magnetic field, *Planet. Space Sci.*, *54*, 153–169.

Choblet, G., and C. Sotin (2000), 3-D thermal convection with variable viscosity: Can transient cooling be described by a quasi-static scaling law?, *Phys. Earth Planet. Inter.*, *119*, 321–336.

Christensen, U. (1984), Heat transport by variable viscosity convection and implications for the Earth's thermal evolution, *Phys. Earth Planet. Inter.*, *35*, 264–282.

Connerney, J. E. P., M. H. Acuña, P. J. Wasilewski, N. F. Ness, H. Reme, C. Mazelle, D. Vignes, R. P. Lin, D. L. Mitchell, and P. A. Cloutier (1999), Magnetic lineations in the ancient crust of Mars, *Science*, *284*, 794–798.

Connerney, J. E. P., M. H. Acuña, N. F. Ness, G. Kletetschka, D. L. Mitchell, R. P. Lin, and H. Reme (2005), Tectonic implications of Mars crustal magnetism, *Proc. Nat. Acad. Sci. U. S. A.*, *102*, 14,970–14,975.

Fowler, A. C., and S. B. G. O'Brien (1996), A mechanism for episodic subduction on Venus, *J. Geophys. Res.*, *101*, 4755–4763.

Fowler, A. C., and S. B. G. O'Brien (2003), Lithospheric failure on Venus, *Proc. R. Soc. London, Ser. A*, *459*, 2663–2704.

Hansen, U., and D. A. Yuen (1989), Subcritical double-diffusive convection at infinite Prandtl number, *Geophys. Astrophys. Fluid Dyn.*, *47*, 199–224.

Hansen, U., and D. A. Yuen (1993), High Rayleigh number regime of temperature-dependent viscosity convection and the Earth's early thermal history, *Geophys. Res. Lett.*, 20, 2191–2194.

Harder, H., and U. Christensen (1996), A one-plume model of Martian mantle convection, *Nature*, 380, 507–509.

Hauck, S. A., and R. J. Phillips (2002), Thermal and crustal evolution of Mars, *J. Geophys. Res.*, 107(E7), 5052, doi:10.1029/2001JE001801.

Karato, S., and P. Wu (1993), Rheology of the upper mantle: A synthesis, *Science*, 260, 771–778.

Karato, S.-I., M. S. Paterson, and J. D. Fitzgerald (1986), Rheology of synthetic olivine aggregates: Influence of grain size and water, *J. Geophys. Res.*, 91, 8151–8176.

Lithgow-Bertelloni, C., and J. H. Guynn (2004), Origin of the lithospheric stress field, *J. Geophys. Res.*, 109, B01408, doi:10.1029/2003JB002467.

Lodders, K., and B. Fegley (1997), An oxygen isotope model for the composition of Mars, *Icarus*, 126, 373–394.

Loddoch, A. (2007), Temporal variations in the convective style of planetary mantles, Ph.D. thesis, Univ. of Münster, Münster, Germany.

Loddoch, A., C. Stein, and U. Hansen (2006), Temporal variations in the convective style of planetary mantles, *Earth Planet. Sci. Lett.*, 251, 79–89.

Moresi, L., and V. Solomatov (1995), Numerical investigation of 2-D convection with extremely large viscosity variations, *Phys. Fluids*, 7, 2154–2162.

Moresi, L., and V. Solomatov (1998), Mantle convection with a brittle lithosphere: Thoughts on the global tectonic styles of the Earth and Venus, *Geophys. J. Int.*, 133, 669–682.

Nataf, H., and F. Richter (1982), Convection experiments in fluids with highly temperature-dependent viscosity and the thermal evolution of the planets, *Phys. Earth Planet. Inter.*, 29, 320–329.

Nimmo, F., and D. J. Stevenson (2000), Influence of early plate tectonics on the thermal evolution and magnetic field of Mars, *J. Geophys. Res.*, 105, 11,969–11,979.

Olson, P. (2003), Thermal interaction of the core and mantle, in *Earth's Core and Lower Mantle*, edited by C. Jones, A. M. Soward, and K. Zhang, pp. 1–29, Taylor and Francis, London.

Patankar, S. V. (1980), *Numerical Heat Transfer and Fluid Flow*, McGraw-Hill, New York.

Ranalli, G. (1987), *Rheology of the Earth: Deformation and Flow Processes in Geophysics and Geodynamics*, Allen and Unwin, Winchester, Mass.

Reese, C., V. Solomatov, and L.-N. Moresi (1998), Heat transport efficiency of stagnant lid convection with dislocation viscosity: Application to Mars and Venus, *J. Geophys. Res.*, 103, 13,643–13,657.

Roberts, G. O. (1977), Fast viscous convection, *Geophys. Astrophys. Fluid Dyn.*, 8, 197–233.

Schubert, G., and T. Spohn (1990), Thermal history of Mars and the sulfur content of its core, *J. Geophys. Res.*, 95, 14,095–14,104.

Schubert, G., D. Turcotte, and P. Olson (2001), *Mantle Convection in the Earth and Planets*, Cambridge Univ. Press, New York.

Sleep, N. (1994), Martian plate tectonics, *J. Geophys. Res.*, 99, 5639–5655.

Smith, D. E., et al. (1998), Topography of the Northern Hemisphere of Mars from the Mars Orbiter Laser Altimeter, *Science*, 279, 1686–1692.

Solomatov, V. S. (1995), Scaling of temperature- and stress-dependent viscosity convection, *Phys. Fluids*, 7, 266–274.

Solomatov, V. S., and L.-N. Moresi (1997), Three regimes of mantle convection with non-Newtonian viscosity and stagnant lid convection on terrestrial planets, *Geophys. Res. Lett.*, 24, 1907–1910.

Solomatov, V. S., and L.-N. Moresi (2000), Scaling of time-dependent stagnant lid convection: Application to small-scale convection on Earth and other terrestrial planets, *J. Geophys. Res.*, 105, 21,795–21,817.

Spohn, T. (1991), Mantle differentiation and thermal evolution of Mars, Mercury, and Venus, *Icarus*, 90, 222–236.

Stein, C., J. Schmalzl, and U. Hansen (2004), The effect of rheological parameters on plate behaviour in a self-consistent model of mantle convection, *Phys. Earth Planet. Inter.*, 142, 225–255.

Steinberger, B., H. Schmeling, and G. Marquart (2001), Large-scale lithospheric stress field and topography induced by global mantle circulation, *Earth Planet. Sci. Lett.*, 186, 75–91.

Stellmach, S., and U. Hansen (2004), Cartesian convection driven dynamos at low Ekman number, *Phys. Rev. E*, 70, 056312, doi:10.1103/PhysRevE.70.056312.

Stevenson, D. J. (2001), Mars' core and magnetism, *Nature*, 412, 214–219.

Stevenson, D. J., T. Spohn, and G. Schubert (1983), Magnetism and thermal evolution of the terrestrial planets, *Icarus*, 54, 466–489.

Tackley, P. (2000a), Self-consistent generation of tectonic plates in time-dependent, three-dimensional mantle convection simulations: 1. Pseudo-plastic yielding, *Geochem. Geophys. Geosyst.*, 1, 1021, doi:10.1029/2000GC000036.

Tackley, P. (2000b), Self-consistent generation of tectonic plates in time-dependent, three-dimensional mantle convection simulations: 2. Strain weakening and asthenosphere, *Geochem. Geophys. Geosyst.*, 1, 1026, doi:10.1029/2000GC000043.

Tanaka, K. L., D. H. Scott, and R. Greeley (1992), Global stratigraphy, in *Mars*, edited by H. Kieffer et al., pp. 345–382, Univ. of Ariz. Press, Tucson.

Travis, B., S. Weinstein, and P. Olson (1990), Three-dimensional convection planforms with internal heat generation, *Geophys. Res. Lett.*, 17, 243–246.

Trompert, R., and U. Hansen (1996), The application of a finite volume multigrid method to three-dimensional flow problems in a highly viscous fluid with a variable viscosity, *Geophys. Astrophys. Fluid Dyn.*, 83, 261–291.

Trompert, R., and U. Hansen (1998a), Mantle convection simulations with rheologies that generate plate-like behaviour, *Nature*, 395, 686–689.

Trompert, R., and U. Hansen (1998b), On the Rayleigh number dependence of convection with a strongly temperature-dependent viscosity, *Phys. Fluids*, 10, 351–360.

Turcotte, D. (1993), An episodic hypothesis for Venusian tectonics, *J. Geophys. Res.*, 98, 17,061–17,068.

Turcotte, D., and G. Schubert (2002), *Geodynamics*, 2nd ed., Cambridge Univ. Press, Cambridge, U. K.

Turcotte, D. L., G. Morein, D. Roberts, and B. D. Malamud (1999), Catastrophic resurfacing and episodic subduction on Venus, *Icarus*, 139, 49–54.

Turner, J. S. (1980), *Buoyancy Effects in Fluids*, Cambridge Univ. Press, Cambridge, U. K.

Wänke, H., and G. Dreibus (1994), Chemistry and accretion history of Mars, *Philos. Trans. R. Soc. London, Ser. A*, 349, 285–293.

Weinstein, S., and P. Olson (1990), Planforms in thermal convection with internal heat sources at large Rayleigh and Prandtl numbers, *Geophys. Res. Lett.*, 17, 239–242.

Wuming, B., C. Vigny, Y. Ricard, and C. Froidevaux (1992), On the origin of deviatoric stresses in the lithosphere, *J. Geophys. Res.*, 97, 11,729–11,737.

Zuber, M. (2001), The crust and mantle of Mars, *Nature*, 412, 220–227.

———————————

U. Hansen, Institute for Geophysics, University of Münster, Corrensstraße 24, D-48149 Münster, Germany.

A. Loddoch, Chevron Energy Technology Company, Technical Computing, 1500 Louisiana Street, Houston, TX 77002, USA. (loddoch@earth.uni-muenster.de)